Thermal-average effects on photoassociation with a slowly-turned-on and rapidly-turned-off laser pulse

Yong-Chang Han,* Jin-Wei Hu, and Bin-Bin Wang
Department of Physics, Dalian University of Technology, Dalian 116024, China

(Received 10 April 2018; revised manuscript received 26 June 2018; published 15 October 2018)

We investigate theoretically the photoassociation (PA) of two Cs atoms using a slowly-turned-on and rapidly-turned-off (STRT) laser pulse at the temperature of 54 μK by taking the thermal average of the initial continuum states into account. For comparison, the PA probabilities under the action of the STRT and typical Gauss-type pulses are calculated, respectively. The rising and falling times of the STRT pulse are set to be $\tau_r = 10$ ps and $\tau_f = 0.2$ ps, and the two Gauss-type pulses are set to be $\tau_r = \tau_f = 10$ ps and $\tau_r = \tau_f = 5.1$ ps, respectively. Compared to the calculation considering a single initial continuum state (non-thermal-average calculations), the PA probabilities with the consideration of the thermal average are reduced to different extents according to different laser pulses. The PA process induced by the STRT pulse is more robust than that by the two Gauss-type pulses. For the STRT pulse, the PA probability is reduced by roughly 30%, while for the two Gauss-type pulses, it is reduced by roughly 97% and 64%, respectively. Because of the larger bandwidth and the asymmetric time profile of the STRT pulse, the PA probability induced by this pulse is related to both the off-resonant and the near-resonant transitions in a much broader phase space formed by the initial continuum states and the final vibrational states. Consequently, the thermal average of the initial continuum states has relatively smaller influence on the PA probability induced by the STRT pulse. By changing the pulse shape of the standard Gaussian to the $\sin^2$ and the Lorentz ones, the STRT pulse still results in the highest PA probability and is the most robust to the thermal average.

DOI: 10.1103/PhysRevA.98.043420

I. INTRODUCTION

The creation and quantum control of cold and ultracold molecules have aroused considerable interest of researchers owing to their wide applications in molecular Bose-Einstein condensation (see, e.g., Ref. [1]), spectroscopy (see, e.g., Ref. [2]), and quantum simulation (see, e.g., Ref. [3]), etc. As one of the prime examples, the photoassociation (PA) process enables us to synthesize cold and ultracold molecules through the interaction of collision atoms with the external laser fields [4–8]. To enhance the yield of associated molecules is one of the most important goals in the PA process and has been studied extensively in both theory and experiment in recent years [9–19]. For instance, the PA yield could be enhanced by properly choosing the parameters of the laser pulse, including carrier frequency, pulse duration, and peak intensity, etc. [20]. It is also proposed that the application of a frequency-chirped pulse could enhance the PA yield [20,21]. The enhancement of the PA yield could also be achieved with a static electric field [22,23]. The PA process could also be manipulated by tuning the scattering length with external magnetic fields [24], or by tuning the relative phase between different coherent association pathways [25]. Another efficient way to improve the PA efficiency is to use the shaped laser pulses (see, e.g., Ref. [26]).

Recently, an asymmetric shaped slowly-turned-on and rapidly-turned-off (STRT) laser pulse has been used to control the molecular orientation in experiments [27–30]. Such an STRT pulse is also adopted to enhance the PA efficiency of Cs atoms [31]. The Cs_2 molecules can be formed by exciting two colliding Cs atoms from the ground electronic state $a\,^3\Sigma_u^+(6S_{1/2}+6S_{1/2})$ to the excited electronic excited state $0_g^-(6S_{1/2}+6P_{3/2})$ with the STRT laser pulse [31]. As shown in Fig. 1, the $0_g^-(6S_{1/2}+6P_{3/2})$ potential has a double-well structure and only the levels in the outer well have relatively larger Franck-Condon (FC) factors with the initial continuum states. Hence, the associated molecules are mainly bound in the outer well. It was shown that a higher PA efficiency can be achieved with the aid of the STRT laser pulse than with a Gauss-type pulse, of which the rising and falling times are set to be the same as the rising time of the STRT pulse [31]. In addition, the PA probability can be further enhanced using a train of STRT laser pulses than that using a train of the Gauss-type pulses [5,32].

In Refs. [5,31,32], two assumptions were applied to the treatment of the initial continuum state for the PA process of two cesium atoms at the ultracold temperature of 54 μK. One assumption was that without consideration of the initial distribution of the collision velocities, the initial state was considered to be totally populated on a single state of which the collision velocity corresponded to the most probable velocity. The other was that only an s wave could contribute to the PA of the two Cs atoms. The former is based on the fact that the velocity distribution is considerably narrow at such an ultracold temperature. The latter assumption is based on the fact that the initial continuum states could not pass the rotational barriers due to the small translational kinetic energy

*Corresponding author: ychan@dlut.edu.cn

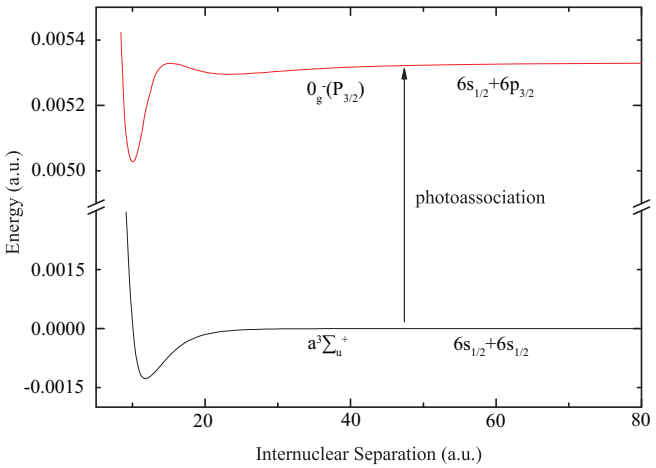

FIG. 1. The relevant potential energy curves and the schematic photoassociation process of the Cs atoms.

for the very low temperatures of ultracold molecules [33,34]. Briefly speaking, no thermal average of the initial continuum states was considered.

However, for the PA induced by a chirped laser pulse, it has been found that the association probability from a thermal average over the incident kinetic energies differs from the probability from a single initial scattering state [20]. Note that the calculation was performed by considering only the s wave. Additionally, besides the s wave, the contribution of higher l waves to the PA probability of Cs atoms induced by the chirped laser pulses is also found to be important in the temperature region from 50 to 150 μK [35]. Thus, even though at the ultracold temperature of $\sim$54 μK, it still needs to be reexamined whether the thermal average over both the incident kinetic energies and the different partial waves could also affect the PA process of the Cs atoms with the STRT laser pulse.

Motivated by these works, we here intend to study the effects of the thermal average of initial continuum states on the PA process induced by an STRT-shaped laser pulse. We are interested to investigate whether the thermal average could also have influence on the PA process induced by the STRT-shaped pulse. If the answer is true, it is further interesting to know how different would it be for the effect of the thermal average on the PA process by the STRT-shaped pulse and that by the traditional unshaped pulses, such as the Gauss-, the $\sin^2$-, and the Lorentz-shaped pulses. In this work, the PA process of two Cs atoms from the $a\,^3\sum_u^+$ to the 0_g^- states at an ultracold temperature of 54 μK is taken as an example. We first take the Gauss-type pulses, for example, and then extend the discussions to the sin2- and the Lorentz-shaped pulses. It is found that the STRT pulses could yield higher PA efficiency when averaged over a thermal distribution of the initial states compared to these standard unshaped pulses. This can be ascribed to the relatively larger bandwidth and the asymmetric time profile of the STRT pulses.

The paper is organized as follows. The theoretical approach is briefly given in Sec. II. The results are described and discussed in detail in Sec. III. A conclusion is drawn in Sec. IV. Atomic units are used throughout the paper, unless specified otherwise.

II. THEORETICAL APPROACH

A. Two-state model

In the Born-Oppenheimer approximation, the interaction of two cesium atoms with an external laser field can be described by the two-state time-dependent Schrödinger equation

$$i\frac{\partial}{\partial t}\begin{pmatrix}\psi_g(R,t)\\ \psi_e(R,t)\end{pmatrix}=\hat{H}\begin{pmatrix}\psi_g(R,t)\\ \psi_e(R,t)\end{pmatrix}, \tag{1}$$

where $\psi_g(R,t)$ and $\psi_e(R,t)$ denote the nuclear wave functions of the ground electronic state $a\,^3\sum_u^+$ and the excited electronic state 0_g^-, respectively. The Hamiltonian describing the transition from $a\,^3\sum_u^+$ to 0_g^- can be expressed as

$$\hat{H}=\begin{pmatrix}\hat{T}+V_g(R) & \hat{W}(t)\\ \hat{W}(t) & \hat{T}+V_e(R)\end{pmatrix}, \tag{2}$$

where $\hat{T}$ is the kinetic-energy operator. $V_g(R)$ and $V_e(R)$ are the potential functions for $a\,^3\sum_u^+$ and 0_g^-, taken from Refs. [36] and [37], respectively.

The interaction $\hat{W}(t)$ is written in the dipole approximation as [35]

$$\hat{W}(t)=-\hat{\varepsilon}(t)\cdot\hat{\mu}(R), \tag{3}$$

where $\hat{\mu}(R)$ is the dipole moment operator. $\varepsilon(t)$ is the time-dependent electric field, which can be expressed as

$$\varepsilon(t)=\varepsilon_0 f(t)\cos[\omega_L(t-t_0)], \tag{4}$$

with

$$f(t)=\exp[-(t-t_0)^2/\tau^2],\quad \tau=\begin{cases}\tau_r(t\leqslant t_0)\\ \tau_f(t>t_0)\end{cases}, \tag{5}$$

where ε_0 is the peak amplitude, t_0 is the corresponding time of the peak amplitude, ω_L is the carrier central frequency, and τ_r and τ_f denote the rising and falling times, respectively. As mentioned above, we consider three different laser pulses, one STRT pulse and two Gauss-type pulses with different durations, respectively, for comparison. These laser pulses are distinguished only by the parameters τ_r and τ_f, and the other laser parameters are set to be the same. We set $\tau_r=10$ ps and $\tau_f=0.2$ ps for the STRT laser pulse, which is the same as the one used in Ref. [31]. If τ_r is set to be equal to τ_f, the laser pulse becomes a typical Gauss-type pulse. Here, two Gauss-type pulses are considered: One is $\tau_r=\tau_f=10$ ps, for which the rising and falling times are the same as the rising time of the STRT pulse, and the other is $\tau_r=\tau_f=5.1$ ps, which has the same area of the time profile as that of the STRT pulse. In order to make a better comparison of these pulses, the electric field in the frequency domain is calculated via Fourier transform:

$$\widetilde{\varepsilon}(\omega)=\int_{-\infty}^{\infty}\varepsilon(t)e^{-i\omega t}dt. \tag{6}$$

In our calculations, we neglect the R dependence of the dipole moment and make use of the asymptotic value, because the photoassociation reaction occurs at a large internuclear

distance. Thus, the interaction $\hat{W}(t)$ can be rewritten as [31]

$$\hat{W}(t) = -W_0 f(t)\cos[\omega_L(t - t_0)], \tag{7}$$

where $W_0 = \varepsilon_0 \mu = 1.0 \times 10^{-5}$ a.u. denotes the interaction intensity at $t = t_0$, and the central frequency ω_L is set to be red detuning from the D_2 atomic resonance line by 3.0 cm^{-1} [31].

B. Thermal average of the initial continuum

There are several methodologies for description of the initial thermal ensemble (see Ref. [35] for ultracold gases and Ref. [38] for the high-temperature case). Here, we follow Ref. [35] for the treatment of the initial thermal ensemble on a finite-size grid, at a temperature $T = 54$ μK. The population is assumed to be initially in the continuum of the ground electronic state at the thermal equilibrium. Given the rotational quantum number l, the Hamiltonian $\hat{H}_g$ of the ground state can be described as

$$\hat{H}_g = -\frac{1}{2u}\frac{\partial^2}{\partial R^2} + V_g(R) + \frac{l(l+1)}{2uR^2}, \tag{8}$$

where u is the reduced mass. The corresponding radial eigenfunctions $\psi_{g,nl}(R)$ and eigenenergy $E_{g,nl}$ can be obtained by diagonalizing $\hat{H}_g$ on a mapped Fourier grid [39,40]. In the calculation, we used 1024 grid points that extend up to 1920 Bohr. n denotes the translational quantum number. As shown in Fig. 1, the dissociation threshold of the ground electronic state is set to be 0. Thus, Eq. (8) gives a spectrum of N_l bound-state solutions at discrete energies $E_{g,nl} < 0$ and $1024 - N_l$ discrete continuum states with $E_{g,nl} > 0$. Instead of labeling those bound states by vibrational quantum number $\nu = 0, 1, ...N_l - 1$ counting up from the bottom of the potential, here we label the bound states by $n = -1, -2, ...$ counting down from the top of the potential for the last, next to last, etc. bond states, and these discrete continuum states are labeled by $n = 1, 2, ...$ counting up from the top of the potential for the lowest, second lowest, etc. Note that the magnetic quantum number m is not lifted by $\hat{H}_g$, and the sum over m can be evaluated, leading to the degeneracy factor $(2l + 1)/4\pi$ [35].

Starting from a given initial continuum state $\psi_{g,nl}(R)$ ($E_{g,nl} > 0$), the corresponding PA probability P_{nl} can be obtained by propagating Eq. (1) from initial time t_i to final time t_f under the action of the laser field,

$$P_{nl} = |\langle\psi_e|\hat{U}(t_f, t_i)|\psi_{g,nl}\rangle|^2, \tag{9}$$

where ψ_e is the excited-state wave function and $\hat{U}(t_f, t_i)$ is the time-evolution operator $\exp[-i\hat{H}t]$ expanded in Chebyshev polynomials [41]. For a detailed description of the solution of the Schrödinger equation, Eq. (1), please refer to Ref. [42].

For a given temperature T, the thermally averaged PA probability is thus given by [35]

$$P_T = \sum_{nl} W_{nl,T} P_{nl}, \tag{10}$$

with the weight factor $W_{nl,T}$ for a specific initial continuum state $\psi_{g,nl}$,

$$W_{nl,T} = \frac{(2l+1)e^{-\beta E_{g,nl}}}{\sum_{nl}(2l+1)e^{-\beta E_{g,nl}}}, \tag{11}$$

where $\beta^{-1} = k_B T$ and k_B is the Boltzmann constant.

It has been checked that the convergence of $W_{nl,T}$ and P_T in Eqs. (10) and (11) can be achieved by summing over $n \in [1, 63]$ and $l \in [0, 100]$, for $T = 54$ μK.

III. RESULTS AND DISCUSSIONS

In this work, to investigate the effect of the thermal average of the initial continuum states on the PA process of the Cs atoms at temperature $T = 54$ μK, we considered three types of laser pulses, as listed in Table I. One is the STRT pulse, which we mainly focused on, and the other two are the Gauss-type laser pules with different durations for comparison. For each pulse, we calculated the PA probability by considering a single initial continuum state, i.e., $P_{\text{single}} = P_{nl}, n = 39, l = 0$, and the PA probability by considering the thermal average of the initial continuum states, i.e., P_T, from Eq. (10). This specific single initial continuum state $\psi_{g,n=39,l=0}$ is the same as the one used in Ref. [5], of which the collision velocity equals the most probable velocity of this system at $T = 54$ μK. The relative variation of the PA probability $|P_{\text{single}} - P_T|/P_{\text{single}}$ is also listed in Table I.

Several aspects could be noted from the data in Table I. First, no matter if we consider the thermal average of the initial continuum or not, the PA probability by the STRT pulse is much greater than those by the Gauss-type pulses by several orders of magnitude. Second, by taking into account the thermal average of initial continuum states, the PA probabilities for the three types of laser pulses are all reduced. Third, the relative variation of the PA probability by the STRT pulse is the smallest. P_T is reduced by roughly 30% with respect to P_{single} for the STRT pulse, while those for the two Gauss-type pulses are reduced by over 90% and 60%, respectively. Thus we can conclude that even at such a low temperature,

TABLE I. The final photoassociation (PA) probability at a temperature of 54 μK for different laser shapes. For each laser parameter, we present the PA probability by considering a single initial continuum state, i.e., $P_{\text{single}} = P_{nl}, n = 39, l = 0$, and the PA probability by considering the thermal average of the initial continuum states, i.e., P_T from Eq. (10). The relative variation of the PA probability $|P_{\text{single}} - P_T|/P_{\text{single}}$ is also listed.

Laser shapes	P_{single}	P_T	$\lvert P_{\text{single}} - P_T\rvert/P_{\text{single}}$
STRT ($\tau_r = 10$ ps, $\tau_f = 0.2$ ps)	2.02×10^{-2}	1.41×10^{-2}	0.30
Gauss-type 1 ($\tau_r = \tau_f = 10$ ps)	9.60×10^{-5}	3.09×10^{-6}	0.97
Gauss-type 2 ($\tau_r = \tau_f = 5.1$ ps)	5.66×10^{-4}	2.03×10^{-4}	0.64

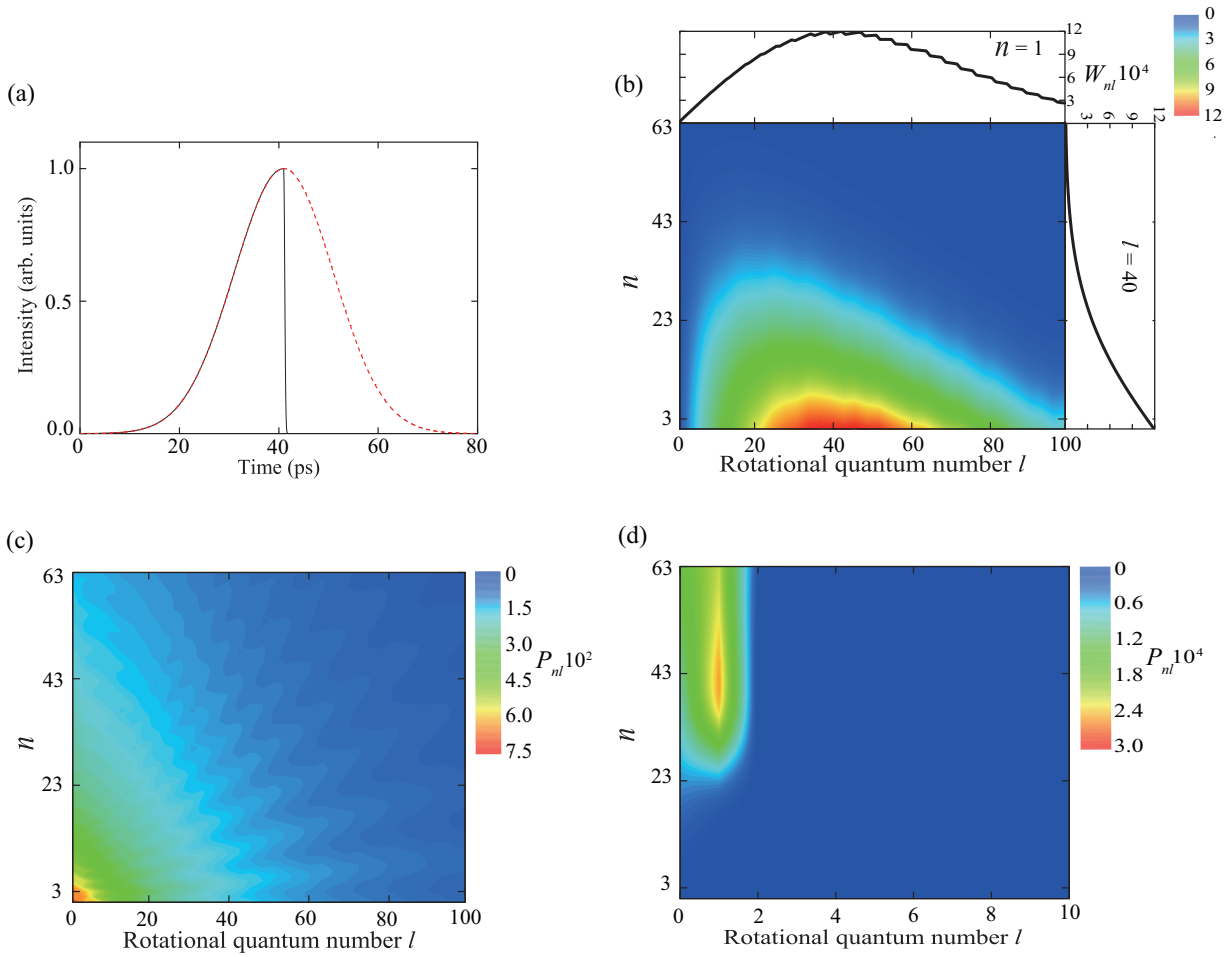

FIG. 2. (a) The time envelopes of the slowly-turned-on and rapidly-turned-off (STRT) laser pulse (black-solid curve) with $\tau_r = 10$ ps and $\tau_f = 0.2$ ps, and the Gauss-type-1 pulse (red-dashed curve) with $\tau_r = \tau_f = 10$ ps. (b) The weight factors W_{nl} for a variety of initial continuum states at a temperature of 54 μK. (c) The PA probabilities for different initial continuum states P_{nl} after the action of the STRT pulse. (d) P_{nl} after the action of the Gauss-type-1 pulse.

$T = 54$ μK, the thermal average of the initial continuum states still has considerable influence on the PA probability. This incoherent average of the initial states could wipe out some of the coherent effects observed in a single initial state and hence the PA probability would be decreased [38]. Nevertheless, the advantage of the STRT pulse is still obvious, for its high PA efficiency and its relative robustness to the thermal average.

To further illustrate the advantage of the STRT pulse in the PA process for an initial thermal ensemble, we first compare the STRT pulse with the Gauss-type-1 pulse in Table I. As shown in Fig. 2(a), because the falling time of the STRT pulse, $\tau_f = 0.2$ ps, is much shorter than that of the Gauss-type-1 pulse, the time profile of the STRT pulse is roughly the first half part of the Gauss-type-1 pulse. For the PA process from a single initial continuum state, the STRT pulse with such a rapid turning-off character can reduce the energy exchange between the molecules and pulse during the falling time period, and consequently, there is not enough energy to transfer the photoassociated molecules from the excited electronic state back to the initial scattering state [31]. As a result, higher PA probability can be obtained by using the asymmetric STRT pulse than by the Gauss-type-1 pulse, for a given initial continuum state. This character could be reserved after the thermal average of the initial continuum state. This is one reason why the STRT pulse enhances the thermally averaged PA efficiency than the Gauss-type pulse.

Moreover, according to Eq. (10), the thermally averaged PA probability is dependent on the weight factor W_{nl} and the PA probability P_{nl} of each initial continuum state, $\psi_{g,nl}$. At $T = 54$ μK, the corresponding weight factors W_{nl} for a variety of initial continuum states are shown in the contour plot of Fig. 2(b). Additionally, to improve the resolution of the contour plot, we added the one-dimensional (1D) plots of W_{nl} for given $n = 1$ and $l = 40$, which are placed on the top and the right sides of the two-dimensional (2D) plot, respectively. It can be seen that for the given "vibrational" label $n = 1$, the weight factor first increases and then decreases with the increasing rotational quantum number l. It is also worth noting that for a fixed quantum number n, the variation of W_{nl} with l is not quite smooth, especially for the large l region. This is because with the increasing l, the associated centrifugal potential increases, and hence the number of the vibrational bound states decreases and that of the discrete continuum states increases. And as mentioned in Sec. II B, we label the discrete continuum states by $n = 1, 2, \ldots$, counting up from

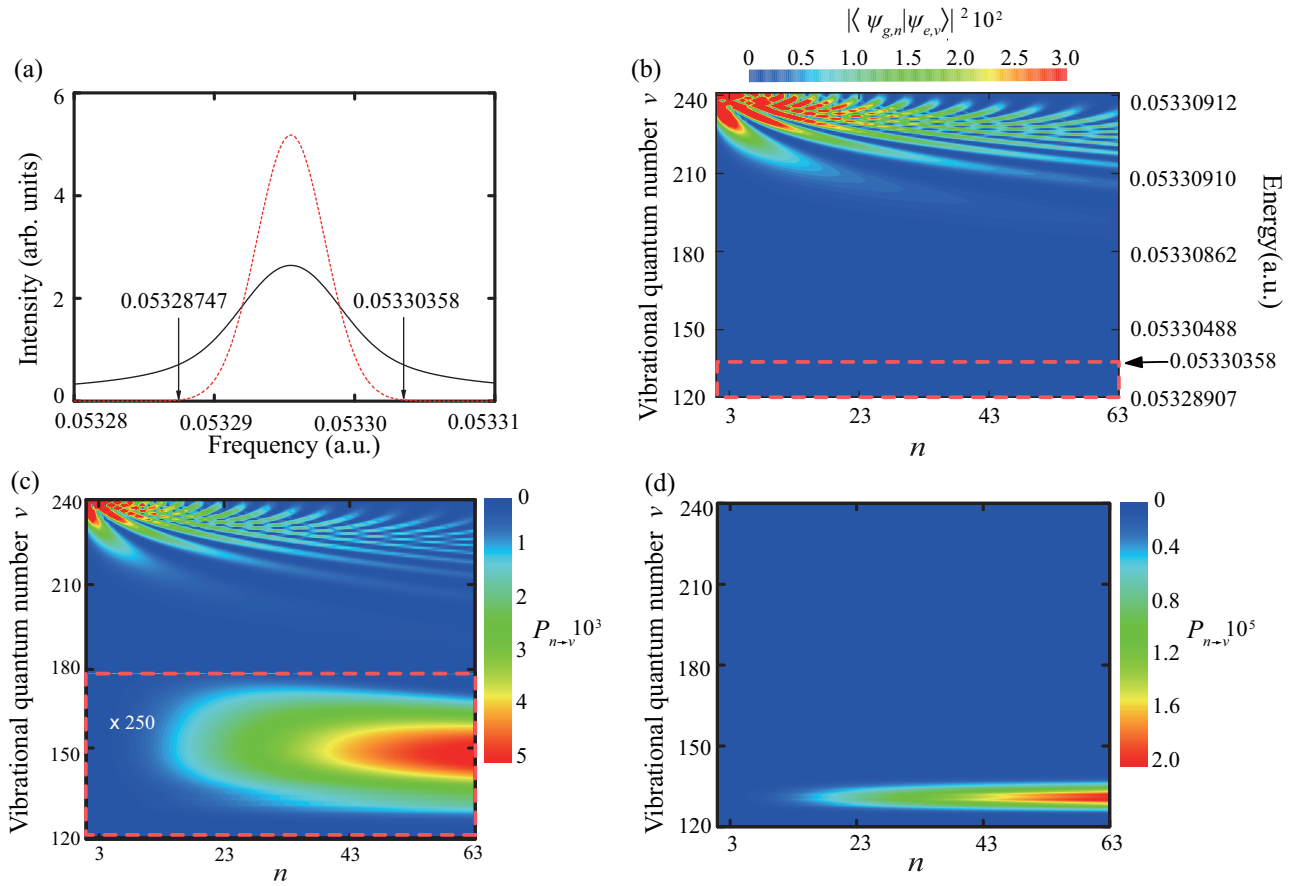

FIG. 3. (a) The electric fields of the laser pulses in the frequency domain for the STRT (black-solid curve) and the Gauss-type-1 (red-dashed curve) pulses, respectively. (b) For $l = 0$, the Franck-Condon factors $|\langle\psi_{g,n}|\psi_{e,v}\rangle|^2$ between the vibrational states of the excited 0_g^- state and the initial continuum states of the ground $a\,^3\Sigma_u^+$ state. The bandwidth of the Gauss-type-1 pulse is marked by the arrows in panel (a), and the corresponding excitation region is marked by the red-dashed frame in panel (b). By fixing the initial rotational quantum number $l = 0$, the transition probability from the initial continuum state n to the vibrational state v, $P_{n\to v}$, is shown in panels (c) and (d) for the STRT pulse and the Gauss-type-1 pulse, respectively. The distribution in the red-dashed frame in panel (c) is zoomed in by the magnification of 250 to be compared with panel (d).

the top of the potential for the lowest, second lowest, etc. Such a treatment leads to the fact that n could only denote the sequence of the discrete continuum states but could not denote the practical "vibrational" mode. Thus, although we use the same n for different l cases, the two quantum states, $\psi_{g,nl}$ and $\psi_{g,nl'}$, may possibly be in different vibrational modes. The larger the number l is, the more possibly this situation occurs. This is consistent with the above findings in the curve W_{nl} versus l, for fixed $n = 1$. Nevertheless, the general trend for the variation of W_{nl} with l still follows the conventional shape of the Boltzmann distribution. For fixed $l = 40$, the weight W_{nl} exponentially decays with n, as shown in the panel on the right side. This is because the effective potential, the sum of the centrifugal potential and the original bare potential, is fixed for a given rotational number, and the corresponding eigenenergy and vibrational mode for the bound vibrational states or the discrete continuum states increase sequentially with the increase of the quantum number n.

From Fig. 2(b), we can see that the weight factors have relatively large magnitudes for the initial states, roughly spanning in the region of $1 \leqslant n \leqslant 20$ and $10 \leqslant l \leqslant 90$. This is an effective region of the initial states $\psi_{g,nl}$. It means that once the initial continuum state $\psi_{g,nl}$ belongs to this region, its contribution P_{nl} to the thermally averaged PA probability P_T would then be considerable. Thus, to obtain an efficient thermally averaged PA probability, two factors are required to be achieved in the meantime: first, the PA probabilities of the given initial states are required to be great enough; second, those initial states are required to fall in the effective region of W_{nl} as much as possible. Additionally, we note that the specific single initial continuum state, which we take as a reference $n = 39, l = 0$ for the calculation of P_{single} in Table I, is out of the effective-weighted region.

Here, we consider the PA probabilities for a variety of initial states P_{nl} after the action of the STRT pulse and the Gauss-type-1 pulse, respectively. As shown in Fig. 2(c), P_{nl}, after the action of the STRT laser pulse, presents a relatively large magnitude ($>3.0 \times 10^{-2}$) in a relatively broad region of $1 \leqslant n \leqslant 23$ and $0 \leqslant l \leqslant 20$. However, for the case of the Gauss-type-1 pulse, the distribution of P_{nl} over the two quantum numbers, n and l, changes dramatically. As seen in Fig. 2(d), not only does the magnitude of P_{nl} decrease entirely by roughly 2 orders, but also the region where P_{nl} is

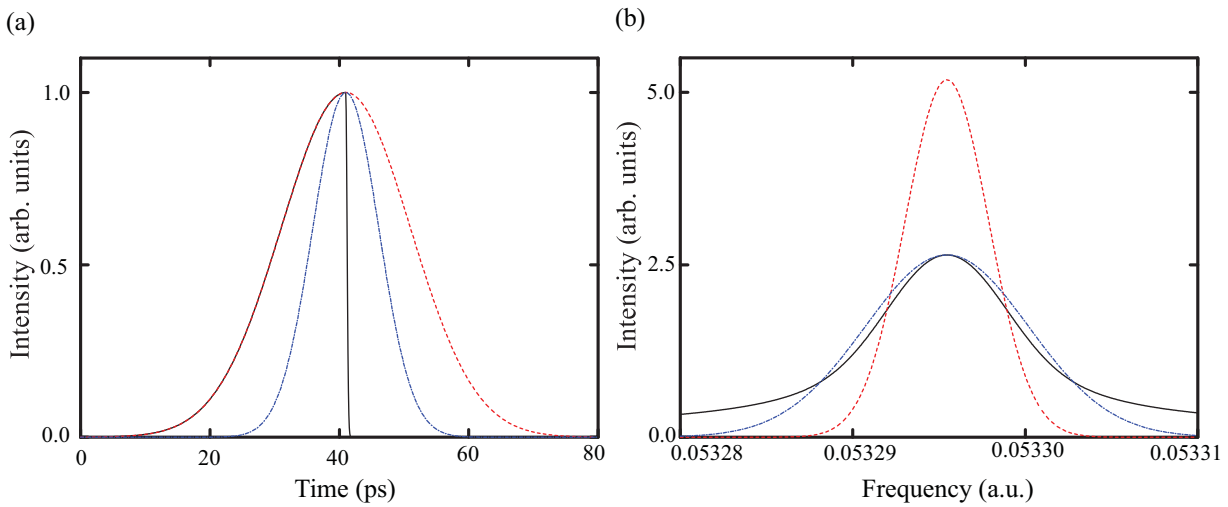

FIG. 4. (a) The time envelopes of the three types of laser pulses: the STRT pulse with $\tau_r = 10$ ps and $\tau_f = 0.2$ ps (black-solid curve), the Gauss-type-1 pulse with $\tau_r = \tau_f = 10$ ps (red-dashed curve), and the Gauss-type-2 pulse with $\tau_r = \tau_f = 5.1$ ps (blue dotted-dashed curve). (b) The corresponding electric fields of these laser pulses in the frequency domain.

dramatically decreases to a small range of $23 \leqslant n \leqslant 63$ and $0 \leqslant l \leqslant 2$. Apparently, under the action of the STRT pulse, a much greater number of initial continuum states could fall into the effective-weighted region and with even higher PA probabilities. Thus, by using the STRT pulse, the two factors mentioned above could be achieved in the meantime. This is the other reason why the STRT pulse could result in a relatively higher thermally averaged PA probability than the Gauss-type-1 pulse.

The asymmetric feature of the STRT pulse in the time domain could enhance the PA probability for a given initial continuum state. As the other side of the coin, the broad distribution of P_{nl} over n and l could be understood from the distribution of the STRT pulse in the frequency domain. The intensity of the electric field as a function of the frequency is shown in Fig. 3(a) for the STRT and the Gauss-type-1 pulses by the black-solid and the red-dashed curves, respectively, which were calculated by Eq. (6). It can be seen that the bandwidth of the STRT pulse in the frequency domain is much broader than that of the Gauss-type-1 pulse, and that the peak amplitude of the electric field in the frequency domain for the STRT pulse is roughly half of that for the Gauss-type-1 pulse. This is consistent with the fact that the area of the STRT pulse in the time domain is roughly half of the Gauss-type-1 pulse. In Fig. 3(b), the Franck-Condon factors $|\langle\psi_{g,n}|\psi_{e,\nu}\rangle|^2$ between the initial discrete continuum states $\psi_{g,n}$ of the ground electronic state and the vibrational states $\psi_{e,\nu}$ of the excited electronic state are shown. Here, we take the case of $l = 0$ as an example. Note that the reference zero energy is set to be the asymptote of the ground electronic state, and the energies for the initial discrete continuum states, $E_{g,n}$, $n \in [1, 63]$, are very dense in energy and very close to the reference zero energy because of the ultracold temperature $T = 54$ K. We thus can consider the energy difference between a specific vibrational state $\psi_{e,\nu}$ and the bunch of initial discrete continuum states $\psi_{g,n}$ to be approximately equal to the corresponding eigenenergy of the state $\psi_{e,\nu}$, as labeled by the side of the right-vertical axis in Fig. 3(b).

Comparing the frequency distribution ranges of the laser pulses in Fig. 3(a) with the energy differences of the upper and lower states in Fig. 3(b), it can be seen that the Gauss-type-1 pulse could couple very finite and relatively deeper vibrational states (ν roughly from 120 to 135) with the initial continuum states, as marked in Fig. 3(b) by the red-dashed frame of which the upper limit is marked by an arrow corresponding to the upper limit of the frequency range of the Gauss-type-1 pulse. Contrarily, the STRT pulse could couple the whole range of the vibrational states shown in Fig. 3(b), i.e., ν from 120 to 240, including the higher vibrational states with significant Franck-Condon factors. These large Franck-Condon factors can guarantee the off-resonant transition to occur, although the electric field intensity of the STRT pulse in this frequency region is relatively weak. The off-resonant transition we mention here is the transition induced by the frequency component which is far beyond the central frequency of the STRT pulse. This could be verified by the vibrational distribution of the electronic excited state after the action of the STRT pulse and the Gauss-type-1 pulse, respectively, as shown in Figs. 3(c) and 3(d). Here, we still fix the initial rotational quantum number $l = 0$, for example, and $P_{n\to\nu}$ denotes the transition probability from the initial continuum state n to the vibrational state ν. It can be seen that because of the broader bandwidth of the STRT pulse and the large Franck-Condon factors in the off-resonant region, those off-resonant transitions to higher vibrational states could contribute a considerable component to the total PA probability. Additionally, in Fig. 3(c), the distribution of $P_{n\to\nu}$ in the red-dashed frame has been zoomed in by the magnification of 250, which is the same scale as that used in Fig. 3(d). Even in the region where the near-resonant transition dominates, the STRT pulse could induce transitions in a relatively broader region. This may be ascribed to the asymmetric character of the time profile of the STRT pulse.

The time profile and the electric field intensity of the Gauss-type-2 pulse are shown in Figs. 4(a) and 4(b), respectively, where the corresponding functions for the STRT and

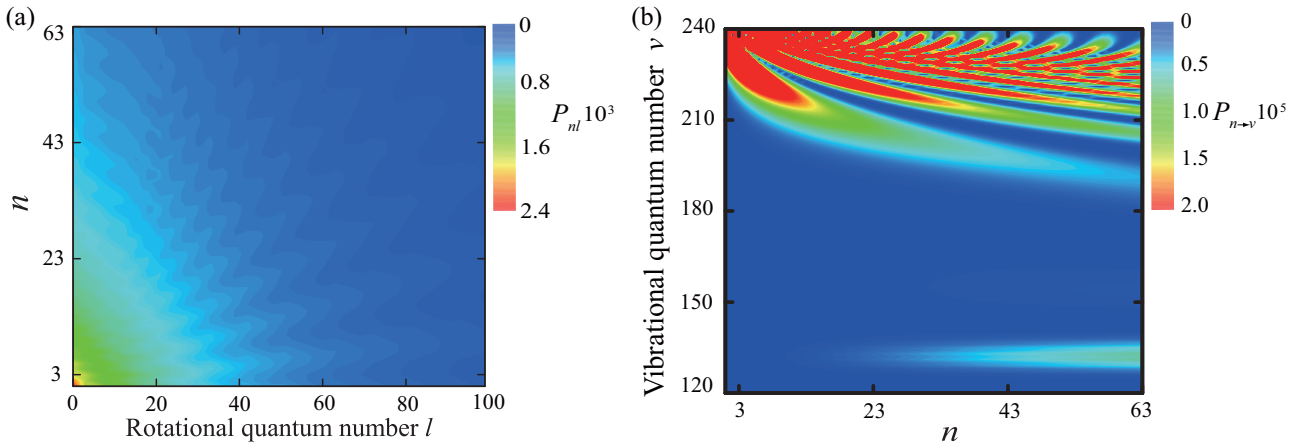

FIG. 5. (a) The PA probabilities for different initial continuum states P_{nl} after the action of the Gauss-type-2 pulse with $\tau_r = \tau_f = 5.1$ ps. (b) By fixing the initial rotational quantum number $l = 0$, the distribution of the transition probability from the initial continuum state n to the vibrational state v, $P_{n\to v}$.

the Gauss-type-1 pulses are also shown for comparison. The area of the time profile of the Gauss-type-2 pulse is set to be the same as the STRT pulse but is symmetric in time. In the frequency domain, the Gauss-type-2 pulse is much broader than the Gauss-type-1 pulse, but its intensity in the off-resonant region is still weaker than the STRT pulse. Thus, the PA probability by this Gauss-type-1 pulse is between that by the STRT pulse and that by the Gauss-type-1 pulse. As shown in Fig. 5(a), the PA probabilities for different initial continuum states P_{nl} by the Gauss-type-1 pulse have a similar distribution character to those by the STRT pulse [Fig. 2(c)], but the magnitude of P_{nl} by the Gauss-type-1 pulse is entirely lower than those by the STRT pulse by roughly 1 order. Moreover, the distribution of $P_{n\to v}$ by the Gauss-type-1 pulse is also similar to that by the STRT pulse [Fig. 3(c)], with contributions from both the off-resonant and the near-resonant transitions; but the scale for Fig. 5(b), which is set to be the same as that used in Fig. 3(d) for the Gauss-type-2 pulse, is much lower than that for Fig. 3(c). It can be seen that by using the Gauss-type-2 pulse, although the off-resonant transition could be induced, the near-resonant transition is however suppressed. Even compared with the case of the Gauss-type-1 pulse, the near-resonant transition induced by the Gauss-type-2 pulse is relatively weaker. Not only is the effective region for the near-resonant transition smaller, but also the magnitude of $P_{n\to v}$ in the near-resonant transition region in Fig. 5(b) is much lower than those in Fig. 3(d).

Now, we could answer the questions addressed at the beginning of this article. Even at the ultracold temperature $\sim$54 μK, the thermal average over the incident kinetic energies and the different partial waves are still required for the three types of pulses we considered here. For the STRT and the Gauss-type-2 pulses which have relatively broader bandwidths, the number of partial waves l is required to be as large as 100 to make the calculation of the thermal average to be converged. Because of the broad bandwidth in frequency domain and the asymmetric character in time, the STRT pulse could induce relatively strong transitions in both the off-resonant and the near-resonant regions, while the Gauss-type-1 pulse with narrow bandwidth could only induce weak near-resonant transitions and the Gauss-type-2 pulse with symmetric character in time could only induce relatively strong off-resonant transitions. This is the reason why the PA probability by the STRT pulse could still remain so high after the thermal average.

Heretofore, the STRT pulse actually can be considered to be a Gauss-type pulse with relatively longer duration which is switched to a much shorter duration. This is why we compare this STRT pulse with the two Gauss-type pulses with different durations. For simplicity, we will refer to this kind of STRT pulse as a STRT-Gauss pulse hereafter. As mentioned above, such an STRT-Gauss pulse is achievable in experiment [27], and the Gaussian time profile used in Eq. (5) has been used for the molecular alignment and orientation [28–30]. It is interesting to investigate whether the other pulse shapes would yield even higher thermally averaged PA yield and whether the STRT pulse generated from the other pulse shapes could still induce high PA probability and still show advantages after the thermal average.

Thus, we further consider another two common types of pulse shapes, the $\sin^2$-shaped and the Lorentz-shaped pulses. The corresponding STRT pulses are named STRT-$\sin^2$ and STRT-Lorentz pulses, respectively, to compare with the STRT-Gauss pulse above. Accordingly, the envelope function $f(t)$ in Eq. (5) is then changed to

$$f(t) = \sin^2\left[\frac{\pi(t-t_0)}{\tau} + \frac{\pi}{2}\right], \quad \tau = \begin{cases} \tau_r \left(t_0 - \frac{\tau_r}{2} \leqslant t \leqslant t_0\right) \\ \tau_f \left(t_0 < t \leqslant t_0 + \frac{\tau_f}{2}\right) \end{cases} \tag{12}$$

for the asymmetric STRT-$\sin^2$ pulse ($\tau_r > \tau_f$) and the symmetric $\sin^2$-shaped pulse ($\tau_r = \tau_f$), and

$$f(t) = \frac{1}{1 + \frac{(t-t_0)^2}{\tau^2}}, \quad \tau = \begin{cases} \tau_r (t \leqslant t_0) \\ \tau_f (t > t_0) \end{cases} \tag{13}$$

for the asymmetric STRT-Lorentz pulse($\tau_r > \tau_f$) and the symmetric Lorentz-shaped pulse ($\tau_r = \tau_f$).

In the calculations, we set the time-profile areas of the STRT-$\sin^2$ and the STRT-Lorentz pulses to be the same

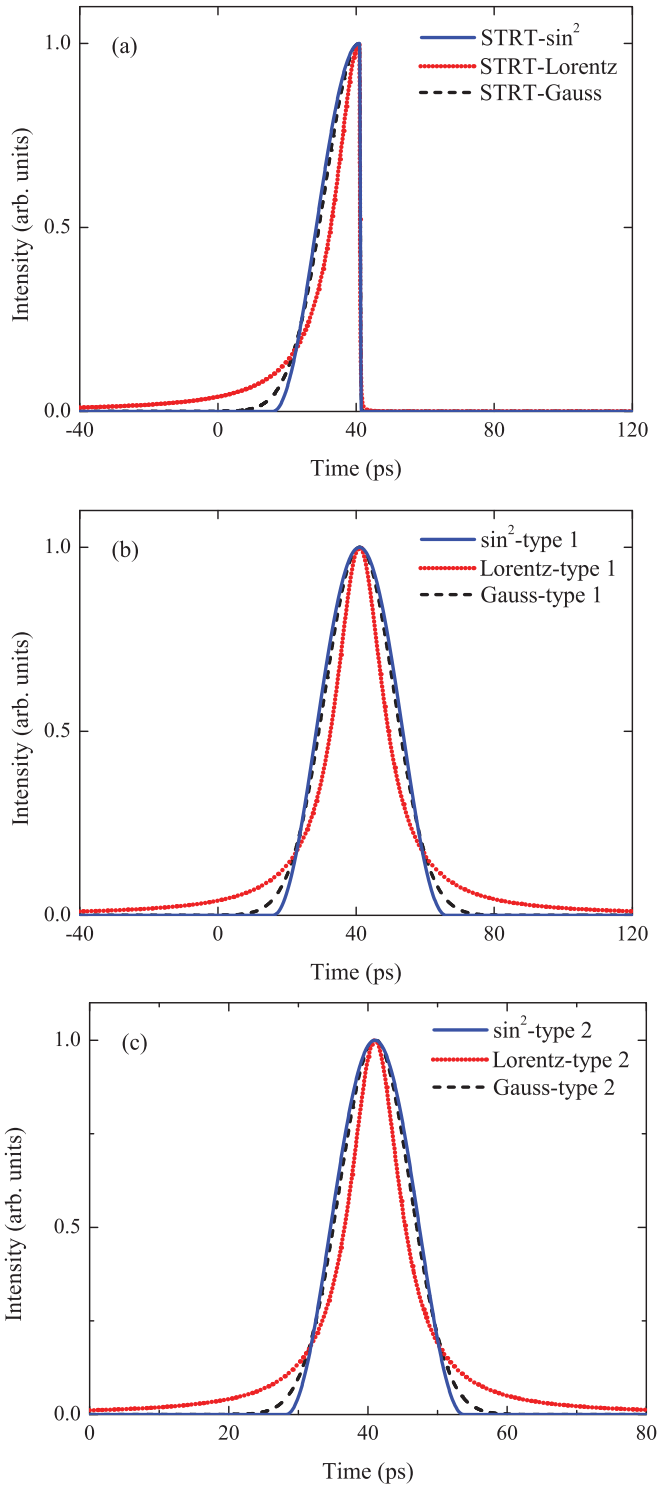

FIG. 6. The time envelopes of (a) the STRT-X, (b) the X-type-1, and (c) the X-type-2 pulses used in Table II. $X = (\sin^2, \text{Lorentz})$. The envelopes of STRT-Gauss, Gauss-type-1, and Gauss-type-2 pulses are also illustrated therein by dashed curves for comparison.

as those of the STRT-Gauss pulse. And for the symmetric $\sin^2$-shaped and Lorentz-shaped pulses, we also consider two types of durations, the longer duration one is set to have the same time-profile area as the Gauss-type-1 pulse, and the shorter one is set to have the same time-profile area as the Gauss-type-2 pulse. The time profiles of these six types of pulses are illustrated in Fig. 6, with the dashed curves denoting the corresponding Gauss-shaped one for comparison. The PA probabilities for these six types of laser pulses, are shown in Table II, with the other laser and molecular parameters the same as Table I. As shown in Table II, the six types of laser pulses are divided into two groups to be compared with Table I. It can be seen that by changing the symmetric Gauss-type pulses and the asymmetric STRT-Gauss pulse into either the $\sin^2$- or the Lorentz-shaped ones, the above conclusions remain the same. Compared to the symmetric X-type ($X = \sin^2$, Lorentz) pulses of two different durations, the STRT-X ($X = \sin^2$, Lorentz) pulse could still result in the highest PA probability and is the most robust to the thermal average. Additionally, as seen in Table II, the absolute values of P_{single} and P_T for the STRT-X ($X = \sin^2$, Lorentz) pulses are very close to those for the STRT-Gauss pulse, while those values for the symmetric X-type ($X = \sin^2$, Lorentz) pulses vary to some extent compared to the corresponding Gauss-type ones. This indicates that the PA probability by the STRT pulse also shows some robustness to the variation of the pulse shapes.

IV. CONCLUSIONS

In summary, we have theoretically investigated the effects of the thermal average of initial continuum states on the photoassociation (PA) process of two Cs atoms at $\sim$54 μK with a slowly-turned-on and rapidly-turned-off (STRT) shaped laser pulse. For comparison, the cases under the action of two typical Gauss-type unshaped laser pulses are also considered. The Gauss-type-1 pulse is narrower in bandwidth, with the rising and falling times to be the same as the slowly-turned-on rising time of the STRT pulse. Such a pulse could only induce near-resonant transition and is the most sensitive to the thermal average. The PA probability has been reduced by roughly 97% after thermal average relative to the non-thermal-average calculations. The Gauss-type-2 pulse, which has the same area of time profile as the STRT pulse, could induce relatively stronger off-resonant transition and rather weaker near-resonant transition. This pulse is also quite sensitive to the thermal average and the PA probability could be reduced by roughly 64%. The STRT pulse works more robustly for the PA process. The corresponding PA probability has only been reduced by roughly 30% after thermal average and still remains a relatively high value, $\sim 1.4 \times 10^{-2}$. The asymmetric time profile and the broad bandwidth of the STRT pulse could guarantee an efficient transition in both the off-resonant and the near-resonant regions. The similar results have been found by changing the pulse shape from the standard Gaussian to the $\sin^2$ and the Lorentz ones. The STRT pulse still results in the highest PA probability and is the most robust to the thermal average. We expect this theoretical investigation could further demonstrate the feasibility for the photoassociation with the STRT laser pulse.

In the present study, to focus on the thermal-average effects on the PA process, we only discussed the formation of the Cs_2 molecules on the excited electronic states from an ensemble of continuum states of the ground electronic state. Further work will estimate more thoroughly whether the target state is selected to be a single state (e.g., the ground vibrational state)

TABLE II. Same as Table I except for another six types of pulse shapes. Here we considered the $\sin^2$-shaped and the Lorentz-shaped pulses, and the STRT pulse based on these two shapes, which is named STRT-X ($X = \sin^2$ or Lorentz), according to Eqs. (12) and (13), respectively. The areas of the time profiles of the STRT-X, the X-type-1, and the X-type-2 pulses are set to be the same as the STRT, the Gauss-type-1, and the Gauss-type-2 pulses used in Table I. The relevant pulse parameters are listed in the parentheses. For comparison, the corresponding data in Table I are also listed in the parentheses.

Laser shapes	P_{single}	P_T	$\lvert P_{\text{single}} - P_T \rvert / P_{\text{single}}$
STRT-$\sin^2$ ($\tau_r = 50.16$ ps, $\tau_f = 1$ ps)	$1.90\ (2.02) \times 10^{-2}$	$1.27\ (1.41) \times 10^{-2}$	0.33 (0.30)
$\sin^2$-type 1 ($\tau_r = \tau_f = 50.16$ ps)	$12.9\ (9.60) \times 10^{-5}$	$5.14\ (3.09) \times 10^{-6}$	0.96 (0.97)
$\sin^2$-type 2 ($\tau_r = \tau_f = 25.56$ ps)	$29.9\ (5.66) \times 10^{-4}$	$11.2\ (2.03) \times 10^{-4}$	0.63 (0.64)
STRT-Lorentz ($\tau_r = 8.375$ ps, $\tau_f = 139$ fs)	$2.19\ (2.02) \times 10^{-2}$	$1.52\ (1.41) \times 10^{-2}$	0.31 (0.30)
Lorentz-type 1 ($\tau_r = \tau_f = 8.375$ ps)	$8.08\ (9.60) \times 10^{-5}$	$2.66\ (3.09) \times 10^{-6}$	0.97 (0.97)
Lorentz-type 2 ($\tau_r = \tau_f = 4.371$ ps)	$27.1\ (5.66) \times 10^{-4}$	$9.68\ (2.03) \times 10^{-4}$	0.64 (0.64)

in the ground electronic state, which is also experimentally aimed. As we mentioned above, after the present photoassociation process, several vibrational states are populated in the excited electronic state of the Cs_2 molecule, which are distributed in both the resonant excitation region and the off-resonant excitation region. It is of significant difficulty to transfer population efficiently from all these vibrational states in the excited electronic state to a single state in the electronic ground state. On one hand, this is a general situation which could be encountered once we achieve the association by pulses of short durations (see, e.g., Ref. [33]). Although the STRT pulse could populate more vibrational states than the Gauss-type pulses could, the STRT pulse still shows efficiency if we consider the single vibrational state, which is also demonstrated in Ref. [5]. Thus, even though we suppose that in a conventional pump-dump scheme, the dumping process could just involve finite vibrational levels in the excited electronic state, it is still highly proposed to adopt the STRT pulse in the first step for the PA process. On the other hand, if it is feasible in experiment, one could consider more control schemes to create molecules in a single state in the ground electronic state. For instance, by using the stimulated Raman adiabatic passage (STIRAP) technique, one could obtain high transfer efficiency to a single state in the ground electronic state (see, e.g., Refs. [43–45]). As the subject of ongoing work, we will consider two pulses of different central frequencies to couple the target ground vibrational state in the ground electronic state with the populated vibrational states in both the resonant and the off-resonant excitation regions, respectively. We will also consider adopting another STRT pulse to achieve a higher transfer efficiency for the dumping process. From this point of view, it is expected that this work could inspire more relevant investigations.

ACKNOWLEDGMENTS

Y.C.H. acknowledges helpful discussions with Xue-Jin Hu, Jing-Lun Li, and Meng Wang. The project was supported by the National Natural Science Foundation of China under Grants No. 21473018 and No. 21873016; the National Key R&D Program of China (No. 2018YFA0306503); the Fundamental Research Funds for the Central Universities (No. DUT18ZD202).

[1] A. S. Peletminskii, S. V. Peletminskii, and Y. V. Slyusarenko, J. Phys. B **50**, 145301 (2017).
[2] M. Ota, H. Tajima, R. Hanai, D. Inotani, and Y. Ohashi, Phys. Rev. A **95**, 053623 (2017).
[3] L. D. Carr, D. DeMille, R. V. Krems, and J. Ye, New. J. Phys. **11**, 055049 (2009).
[4] T. Mullins, W. Salzmann, S. Götz, M. Albert, J. Eng, R. Wester, M. Weidemüller, F. Weise, A. Merli, S. M. Weber, F. Sauer, L. Wöste, and A. Lindinger, Phys. Rev. A **80**, 063416 (2009).
[5] W. Zhang, G.-R. Wang, and S.-L. Cong, Phys. Rev. A **83**, 045401 (2011).
[6] A. T. Krupp, A. Gaj, J. B. Balewski, P. Ilzhöfer, S. Hofferberth, R. Löw, T. Pfau, M. Kurz, and P. Schmelcher, Phys. Rev. Lett. **112**, 143008 (2014).
[7] K. M. Jones, E. Tiesinga, P. D. Lett, and P. S. Julienne, Rev. Mod. Phys. **78**, 483 (2006).
[8] B.-B. Wang, Y.-C. Han, and S.-L. Cong, J. Chem. Phys. **143**, 094303 (2015).
[9] M. Machholm, A. Giusti-Suzor, and F. H. Mies, Phys. Rev. A **50**, 5025 (1994).
[10] H. M. J. M. Boesten, C. C. Tsai, D. J. Heinzen, A. J. Moonen, and B. J. Verhaar, J. Phys. B **32**, 287 (1999).
[11] F. Fatemi, K. M. Jones, H. Wang, I. Walmsley, and P. D. Lett, Phys. Rev. A **64**, 033421 (2001).
[12] W. Salzmann, U. Poschinger, R. Wester, M. Weidemüller, A. Merli, S. M. Weber, F. Sauer, M. Plewicki, F. Weise, A. M. Esparza, L. Woste, and A. Lindinger, Phys. Rev. A **73**, 023414 (2006).
[13] C. Haimberger, J. Kleinert, O. Dulieu, and N. P. Bigelow, J. Phys. B **39**, S957 (2006).
[14] M. Pichler, W. C. Stwalley, and O. Dulieu, J. Phys. B **39**, S981 (2006).
[15] P. Shen, Y.-C. Han, J.-L. Li, K. Yi, C. Chen, and S.-L. Cong, Laser Phys. Lett. **12**, 045302 (2015).
[16] Y.-C. Han, Laser Phys. Lett. **14**, 125302 (2017).
[17] J. Pérez-Rios, M. Lepers, and O. Dulieu, Phys. Rev. Lett. **115**, 073201 (2015).

[18] S. Taie, S. Watanabe, T. Ichinose, and Y. Takahashi, Phys. Rev. Lett. **116**, 043202 (2016).
[19] C. Chandre, J. Mahecha, and J. P. Salas, Phys. Rev. A **95**, 033424 (2017).
[20] E. Luc-Koenig, M. Vatasescu, and F. Masnou-Seeuws, Eur. Phys. J. D **31**, 239 (2004).
[21] J. L. Carini, S. Kallush, R. Kosloff, and P. L. Gould, Phys. Rev. Lett. **115**, 173003 (2015).
[22] D. Chakraborty, J. Hazra, and B. Deb, J. Phys. B **44**, 095201 (2011).
[23] D. Chakraborty and B. Deb, AIP Adv. **4**, 017134 (2014).
[24] G. Feng, Y. Li, X. Wang, J. Wu, V. B. Sovkov, J. Ma, L. Xiao, and S. Jia, Sci. Rep. **7**, 13677 (2017).
[25] E. F. de Lima, Phys. Rev. A **95**, 013411 (2017).
[26] L. Levin, W. Skomorowski, R. Kosloff, C. P. Koch, and Z. Amitay, J. Phys. B **48**, 184004 (2015).
[27] B. J. Sussman, J. G. Underwood, R. Lausten, M. Yu. Ivanov, and A. Stolow, Phys. Rev. A **73**, 053403 (2006).
[28] Y. Sugawara, A. Goban, S. Minemoto, and H. Sakai, Phys. Rev. A **77**, 031403 (2008).
[29] M. Muramatsu, M. Hita, S. Minemoto, and H. Sakai, Phys. Rev. A **79**, 011403 (2009).
[30] A. Goban, S. Minemoto, and H. Sakai, Phys. Rev. Lett. **101**, 013001 (2008).
[31] W. Zhang, Y. Huang, T. Xie, G.-R. Wang, and S.-L. Cong, Phys. Rev. A **82**, 063411 (2010).
[32] Y. Hai, X.-J. Hu, J.-L. Li, and S.-L. Cong, Mol. Phys. **115**, 1984 (2017).
[33] E. Luc-Koenig, R. Kosloff, F. Masnou-Seeuws, and M. Vatasescu, Phys. Rev. A **70**, 033414 (2004).
[34] A. Crubellier and E. Luc-Koenig, J. Phys. B **39**, 1417 (2006).
[35] C. P. Koch, E. Luc-Koenig, R. Kosloff, F. Masnou-Seeuws, and A. Crubellier, J. Phys. B **39**, S1017 (2006).
[36] D. Comparat, C. Drag, B. Laburthe Tolra, A. Fioretti, P. Pillet, A. Crubellier, O. Dulieu, and F. Masnou-Seeuws, Eur. Phys. J. D **11**, 59 (2000).
[37] J. Vala, O. Dulieu, F. Masnou-Seeuws, P. Pillet, and R. Kosloff, Phys. Rev. A **63**, 013412 (2000).
[38] S. Amaran, R. Kosloff, M. Tomza, W. Skomorowski, F. Pawłowski, R. Moszynski, L. Rybak, L. Levin, Z. Amitay, J. Martin Berglund, D. M. Reich, and C. P. Koch, J. Chem. Phys. **139**, 164124 (2013).
[39] V. Kokoouline, O. Dulieu, R. Kosloff, and F. Masnou-Seeuws, J. Chem. Phys. **110**, 9865 (1999).
[40] K. Willner, O. Dulieu, and F. Masnou-Seeuws, J. Chem. Phys. **120**, 548 (2004).
[41] R. Kosloff, J. Phys. Chem. **92**, 2087 (1988).
[42] M. Wang, J.-L. Li, X.-J. Hu, M.-D. Chen, and S.-L. Cong, Phys. Rev. A **96**, 043417 (2017).
[43] F. Lang, K. Winkler, C. Strauss, R. Grimm, and J. Hecker Denschlag, Phys. Rev. Lett. **101**, 133005 (2008).
[44] Z. F. Feng, W. D. Li, L. R. Wang, L. T. Xiao, and S. T. Jia, Phys. Rev. A **80**, 043620 (2009).
[45] X.-J. Hu, W. Zhang, Y. Huang, J.-F. Yang, and S.-L. Cong, J. Theor. Comput. Chem. **11**, 1323 (2012).